

Quantum Coherence in Photo-Ionization with Tailored XUV Pulses

Stefanos Carlström^{1,*}, Johan Mauritsson¹, Kenneth J. Schafer², Anne L’Huillier¹,
and Mathieu Gisselbrecht^{1,†}

¹*Department of Physics, Lund University, Box 118, 221 10 Lund, Sweden*

²*Department of Physics and Astronomy, Louisiana State University, Baton Rouge, LA 70803*

**Email: stefanos.carlstrom@gmail.com*

†*Email: mathieu.gisselbrecht@sljus.lu.se*

December 14, 2024

Abstract

Ionization with ultrashort pulses in the extreme ultraviolet (XUV) regime can be used to prepare an ion in a superposition of spin-orbit substates. In this work, we study the coherence properties of such a superposition, created by ionizing xenon atoms using two phase-locked XUV pulses at different frequencies. In general, if the duration of the driving pulse exceeds the quantum beat period, dephasing will occur. If however, the frequency difference of the two pulses matches the spin-orbit splitting, the coherence can be efficiently increased and dephasing does not occur.

1 INTRODUCTION

The wave nature of matter is central to the quantum mechanical description of the microcosmos; therefore coherence is an important property of any quantum system. An example of a coherent system is the superposition of two pure states, $|\psi\rangle = a|1\rangle + b|2\rangle$; such superpositions form the basis for the field of quantum information, where they are used to represent qubits. The manipulation of qubits for quantum computing necessarily requires that the coherence of the system is retained; if not, the information contained within the qubit is lost. In quantum optics, superpositions between two states may be created via a transition between the two states with an appropriately tailored pulse (e.g. a $\pi/2$ -pulse) [figure 1 (a)].

Superpositions of states can also be achieved by direct excitation using short light pulses [figure 1 (b)], provided the bandwidth of the pulse is larger than the energy difference (ω_{21}) between the two states. This requires a pulse duration short enough, $\tau \leq 2\pi/\omega_{21}$. If the superposition is successfully created, it may be observed through quantum beats (Teets et al. 1977; Salour and Cohen-Tannoudji 1977; Mauritsson et al. 2010; Tzallas et al. 2011) which usually last substantially longer than the pulse duration. The characteristic decay time is termed the *coherence time*. In the cases depicted in 1 (a) and (b), the light couples the bound states and enables coherent population transfer.

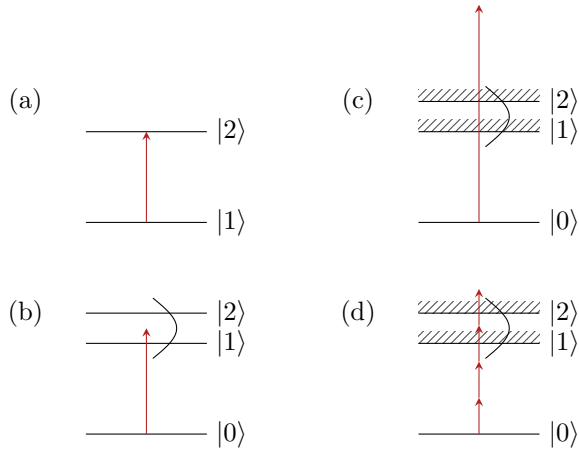


FIGURE 1: Different ways of preparing coherent superpositions using light; (a) excitation of a two-level system, such as those used for qubits in quantum information; (b) coherent excitation from the ground state to two excited bound states; (c) single-photon ionization, with the ion left in a superposition of substates; (d) strong-field ionization, also leaving the ion in a superposition of substates.

Another way to produce a superposition of states is via short-pulse ionization, when the ion is left in a coherent superposition of final states, e.g. due to spin-orbit interaction. This can be done using either high-frequency [figure 1 (c)] or high-intensity short-pulse [figure 1 (d)] radiation. As previously, the bandwidth of the ionizing pulse has to exceed the energy splitting between the ion states. Kurka et al. (2009) investigated case 1 (c) by photo-ionizing neon using short XUV pulses from a free-electron laser. A coherent superposition of the ionic fine-structure substates was prepared and probed by subsequent ionization. Using a strong laser field [figure 1 (d)], Goulielmakis et al. (2010) photo-ionized krypton, leaving the residual Kr^+ ion in a coherent superposition of the ionic substates. The quantum beat was observed by probing with a delayed attosecond (as) XUV pulse. This experimental activity stimulated an important theoretical effort to investigate the coherence of superpositions of states produced either directly by photo-excitation [figure 1 (b); Tzallas et al. 2011; Klünder et al. 2013], single-photon ionization [figure 1 (c); Nikolopoulos 2013], or strong-field ionization [figure 1 (d); Pabst et al. 2011, 2016].

In this article, we present a theoretical study of single-photon ionization of a rare gas using tailored XUV pulses. We use two phase-locked pulses of different frequencies (e.g. two high-order harmonics), to ionize xenon atoms, leaving the ion in a superposition of the $5\text{p}^5 \ ^2\text{P}_{3/2,1/2}^o$ ionic substates (figure 2). When the frequency difference between the two pulses equals the spin-orbit splitting, the coherence can be retained, in principle, indefinitely. This resonance condition corresponds to a situation where two quantum paths lead to the same photo-electron state. We investigate the tolerance of this resonance condition, i.e. how strict is the requirement on the excitation frequencies and pulse duration of the driving field for maintaining a certain level of coherence? Our method is based on an exact solution of the time-dependent Schrödinger equation using a fully correlated atomic model and assuming weak-field (perturbative) ionization. The coherence of the quantum system is analyzed using the density matrix formalism.

This paper is organized as follows; in the following section, the model is presented, along with the tools that are used to calculate the evolution of the superposition of states in the presence of the driving field. We then present the results and conclude with a discussion. Atomic units are used throughout, unless otherwise stated.

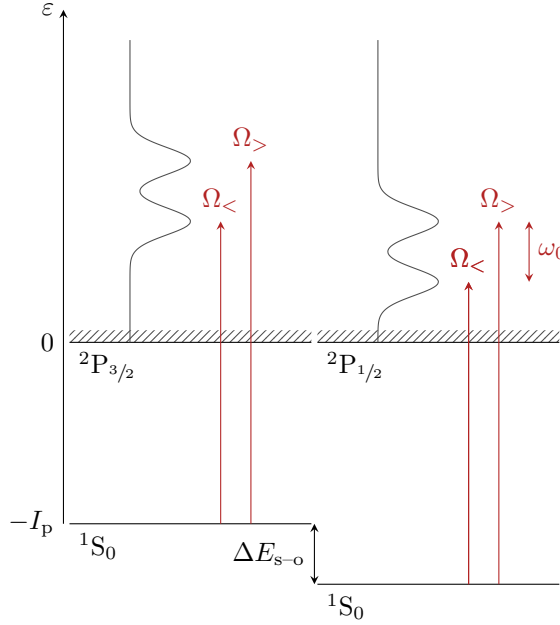


FIGURE 2: Schematic energy diagram of a noble gas (heavier than He, i.e. with a spin-orbit splitting of the first ionic ground state $np^5 2P_{j_i}$, $j_i = 3/2, 1/2$) photo-ionized with a tailored XUV pulse consisting of two frequencies with $\Omega_> - \Omega_< = \omega_0$. The energy scale is that of the photo-electron kinetic energy, which depends on the final ion state, $2P_{3/2}$ or $2P_{1/2}$. It can be seen from the diagram that there are four pathways to the continuum. If $\omega_0 \approx \Delta E_{s-o}$, two of the quantum paths (absorption of $\Omega_<$ and the ion in $2P_{3/2}$; absorption of $\Omega_>$ and the ion in $2P_{1/2}$) lead to the same photo-electron energy.

2 THEORETICAL FRAMEWORK

We are interested in studying the coherence of different ionic states produced by photo-ionization with tailored XUV pulses. To this end, we use as a model system noble gas ions, which have a spin-orbit splitting of the ground state ($np^5 2P_{j_i}^0$, $j_i = 3/2, 1/2$), in particular xenon ($n = 5$).

Figure 2 shows a simplified diagram of photo-ionization of a np electron. The ionic ground state has a spin-orbit splitting, which in xenon is 1.3 eV. We ionize with a weak XUV pulse with two frequency components, whose difference is ω_0 . Absorption of the two frequency components, $\Omega_>$ and $\Omega_<$, leads to an ion in either $2P_{3/2}^0$ or $2P_{1/2}^0$, resulting in four different pathways. If the frequency difference is equal to the spin-orbit spacing, there will be two (indistinguishable) pathways to the same final photo-electron energy; we call this the *resonant case*. We introduce the *detuning ratio* $d \equiv \omega_0 / \Delta E_{s-o}$, and study photoionization in the vicinity of this resonance ($d \approx 1$).

The calculations are performed by solving the time-dependent Schrödinger equation (TDSE) in a limited subspace,

$$i \frac{\partial}{\partial t} |\Psi(t)\rangle = \mathcal{H}(t) |\Psi(t)\rangle, \quad (1)$$

where the Hamiltonian in the dipole approximation is

$$\mathcal{H}(t) = \mathcal{H}_0 + \mathcal{E}(t) z. \quad (2)$$

\mathcal{H}_0 is the atomic Hamiltonian, $\mathcal{E}(t)$ the electric field, and z is the dipole operator for linear polarization along the z axis. The solution is found by propagating the initial state (the neutral ground state) to time t

$$|\Psi(t)\rangle = \mathcal{U}(t, 0) |\Psi_0\rangle, \quad (3)$$

TABLE 1: Ionization channels accessible via one-photon ionization from the valence shell of a noble gas (final $J = 1$), in the case of jK coupling.

Nº	Channel configuration
1	$np^5(^2P_{3/2}^o)kd\ ^2[1/2]_1$
2	$np^5(^2P_{3/2}^o)ks\ ^2[3/2]_1$
3	$np^5(^2P_{3/2}^o)kd\ ^2[3/2]_1$
4	$np^5(^2P_{1/2}^o)ks\ ^2[1/2]_1$
5	$np^5(^2P_{1/2}^o)kd\ ^2[3/2]_1$
6	$nsnp^6(^2S_{1/2})kp\ ^2[1/2]_1$
7	$nsnp^6(^2S_{1/2})kp\ ^2[3/2]_1$

where the short-time propagator is approximated by a Magnus (1954) propagator of fourth order (Saad 1992; Alvermann et al. 2012).

The basis functions and the dipole matrix elements are determined using ATSP2K (multi-configurational Hartree–Fock; Froese Fischer et al. 2007) and BSR (close-coupling R -matrix approach; Zatsarinsky 2006; Zatsarinsky and Froese Fischer 2009). The time-dependent wavefunction is expanded as

$$|\Psi(t)\rangle = c_0(t)|\Psi_0\rangle + \sum_i \sum_\ell \int d\varepsilon c_i^\ell(t; \varepsilon)|i\varepsilon\ell\rangle, \quad (4)$$

where $|\Psi_0\rangle$ is the ground state $ns^2np^6\ ^1S_0$, $c_0(t)$ the complex, time-dependent amplitude, i denotes the final state of the ion, and $\varepsilon\ell$ the quantum state of the photo-electron with angular momentum ℓ and energy ε (related to the momentum k by $\varepsilon = k^2/2$). The ionization channels formed by different possible combinations of i and ℓ , are listed in table 1, in the case of jK coupling. jK (or pair) coupling is defined as (Cowan 1981) $\mathbf{j}_i + \boldsymbol{\ell} = \mathbf{K}$ and $\mathbf{K} + \mathbf{s} = \mathbf{J}$, where \mathbf{j}_i is the total angular momentum of the parent ion, which couples to the angular momentum of the electron $\boldsymbol{\ell}$ to form an intermediate \mathbf{K} . The levels are then written as $\gamma_i(^{2S+1}L_{j_i})k\ell\ ^{2S+1}[K]_J$, where γ_i is the electron configuration of the ion.

In the field-free basis, \mathcal{H}_0 is simply a diagonal matrix, with the energies of the photo-electron with respect to the lowest ionization threshold as matrix elements. In the weak-field limit, the partial-wave expansion is restricted to total angular momentum $J \leq 1$, i.e. no multi-photon processes are considered. Furthermore, ionization is only allowed from the outer np shell (photo-electron energies in the range 0 eV to 11 eV in the case of xenon), to avoid autoionization of embedded Rydberg states in the vicinity of the $nsnp^6\ ^2S_{1/2}$ threshold (that is, channels 6 and 7 in table 1 need not be considered). We also neglect mixing of singlet and triplet terms. Thus, the only non-zero matrix elements of the dipole operator z are $\langle i\varepsilon\ell|z|\Psi_0\rangle$ (and the complex conjugate), which are spin-averaged by BSR.

The analysis of the coherence is made using the density matrix formalism [Landau and Lifshitz 1977, §14], where the full *density matrix* operator is defined as (time dependence t omitted for brevity)

$$\rho_T = |\Psi\rangle\langle\Psi|, \quad (5)$$

with matrix elements of the continuum block

$$\rho_{i_1 i_2}^{\ell_1 \ell_2}(\varepsilon_1, \varepsilon_2) \equiv c_{i_1}^{\ell_1}(\varepsilon_1) c_{i_2}^{\ell_2*}(\varepsilon_2). \quad (6)$$

We reduce this density matrix to an ion–channel density matrix by first taking the trace over the photo-electron energy ε :

$$\begin{aligned}\rho_{i_1 i_2}^{\ell_1 \ell_2} &\equiv \int d\varepsilon \langle \varepsilon | \Psi \rangle \langle \Psi | \varepsilon \rangle = \int d\varepsilon \sum_{i_1 i_2} \sum_{\ell_1 \ell_2} \int d\varepsilon_1 d\varepsilon_2 \langle \varepsilon | i_1 \varepsilon_1 \ell_1 \rangle c_{i_1}^{\ell_1}(\varepsilon_1) c_{i_2}^{\ell_2*}(\varepsilon_2) \langle i_2 \varepsilon_2 \ell_2 | \varepsilon \rangle \\ &= \sum_{i_1 i_2} \sum_{\ell_1 \ell_2} \int d\varepsilon |i_1 \ell_1 \rangle \rho_{i_1 i_2}^{\ell_1 \ell_2}(\varepsilon, \varepsilon) \langle i_2 \ell_2 |.\end{aligned}\quad (7)$$

Finally, we construct the ion density matrix by tracing over the photo-electron angular momenta:

$$\rho_{i_1 i_2} \equiv \sum_{\ell} \sum_{i_1 i_2} \sum_{\ell_1 \ell_2} \langle \ell | i_1 \ell_1 \rangle \rho_{i_1 i_2}^{\ell_1 \ell_2} \langle i_2 \ell_2 | \ell \rangle = \sum_{\ell} \sum_{i_1 i_2} |i_1 \rangle \rho_{i_1 i_2}^{\ell \ell} \langle i_2 |. \quad (8)$$

The diagonal elements (ρ_{mm}) of this matrix are the populations in each of the ionic states, while the off-diagonal elements (ρ_{mn}) contain the coherences between the ionic states. The only non-zero off-diagonal elements are those corresponding to channels for which all quantum numbers are the same (except for the angular momentum of the ion); i.e. only $\rho_{35} = \rho_{53}^* \neq 0$. Decoherence due to the spin–orbit interaction is neglected.

3 RESULTS

We investigate the real-time build-up of coherence with a XUV pulse of short or long duration in the non-resonant case (figure 3, left) and the resonant case (figure 3, right). The electromagnetic fields are presented in the upper panels. In both cases, they consist of harmonics 13 & 14 of a fundamental driving field. The short-pulse duration is 500 as, while the long-pulse duration is 15 fs resulting in the formation of a periodic beating of the XUV pulse. Regardless of the pulse duration, the population in the ionic substates (middle shown in solid and dashed lines) increases as the pulse ionizes the atom. The population is proportional to the integral of the pulse intensity, hence the appearance of steps in the population.

3.1 The non-resonant case

We first consider the non-resonant case (left panels of figure 3), where the fundamental driving frequency is $\omega_0 = 1.3\Delta E_{\text{s-o}}$. For a short pulse duration, the coherence increases during the interaction and stays constant after the pulse has passed. In contrast, for long pulse duration, the coherence first builds up, and then vanishes at the end of the pulse. The decoherence time, i.e. the time from the onset of the pulse to the decrease of the coherence (see lower panel of figure 3), is approximately equal to the quantum beat period $T = 2\pi/\Delta E_{\text{s-o}}$ of the ionic substates; for xenon with a spin–orbit splitting of 1.3 eV, it is 3.2 fs.

3.2 The resonant case

In the resonant case (right panels of figure 3), the situation is completely different. The coherence is built up during all the interaction time, and remains after the end of the pulse. The existence of this resonant condition can be understood by considering the population of the ionic substates

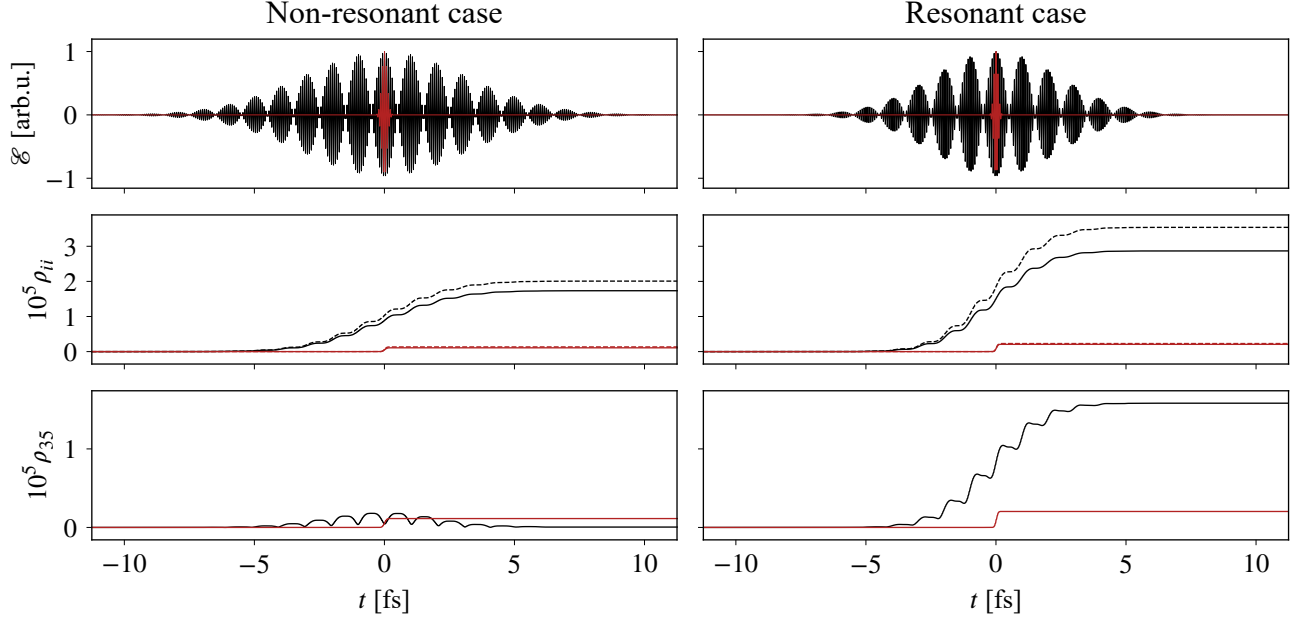


FIGURE 3: Real-time coherence build-up, for the case of ionization with two harmonics, 13 and 14 of a fundamental frequency $d\Delta E_{\text{s-o}}$, in the non-resonant case ($d = 1.3$) left and the resonant case ($d = 1$) right. The upper panels show the driving fields used; the red curve corresponds to a pulse duration (FWHM of the temporal intensity profile) of 500 fs while the black curve corresponds to a pulse duration of 15 fs. The middle panels show the populations in the residual ionic substates (solid: contribution from channel 3 to $^2\text{P}_{3/2}^o$; dashed: contribution from channel 5 to $^2\text{P}_{1/2}^o$), which increase with time. The lower panels show the induced coherence between the ionic substates, which is built up over time. For the short-pulse case, there is always coherence left at the end of the pulse, while for the longer pulse duration, the resonance criterion has to be fulfilled $d \approx 1$ for this to happen. The lower population in the non-resonant case is explained by the decrease in photoionization cross-section with increasing photon energy.

(labelled $|1\rangle$ and $|2\rangle$, for simplicity) resulting from a periodic sequence of ionization events occurring at times t_k ($k \in \mathbb{N}$). The wavefunction is then

$$|\Psi(t_1)\rangle = c_1(t_1)e^{i\phi_{\text{XUV}}(t_1)}|1\rangle + c_2(t_1)e^{i\phi_{\text{XUV}}(t_1)}|2\rangle, \quad (9)$$

where ϕ_{XUV} is the phase of the ionizing XUV field at time t_1 . At the k th event, the wavefunction becomes

$$|\Psi(t_k)\rangle = c_1(t_k)e^{i\phi_{\text{XUV}}(t_k)}|1\rangle + c_2(t_k)e^{i\phi_{\text{XUV}}(t_k)}|2\rangle + \mathcal{U}(t_k, t_{k-1})|\Psi(t_{k-1})\rangle, \quad (10)$$

where $\mathcal{U}(t_k, t_{k-1})$ propagates the wavefunction from an earlier time step. The propagator can be written

$$\mathcal{U}(t_k, t_{k-1}) = \exp(-i\mathcal{H}\Delta t), \quad (11)$$

where the Hamiltonian matrix (assuming no spin-orbit coupling) is

$$\mathcal{H} = \begin{pmatrix} E_1 & 0 \\ 0 & E_2 \end{pmatrix}, \quad (12)$$

and $\Delta t \equiv t_k - t_{k-1}$ is the separation between the ionization events. Finally, the wavefunction reads as

$$|\Psi(t_k)\rangle = \sum_{a=1}^k c_1(t_a)e^{i[\phi_{\text{XUV}}(t_a) - E_1(k-a)\Delta t]} [|1\rangle + \tilde{c}e^{-i\Delta E\Delta t(k-a)}|2\rangle], \quad (13)$$

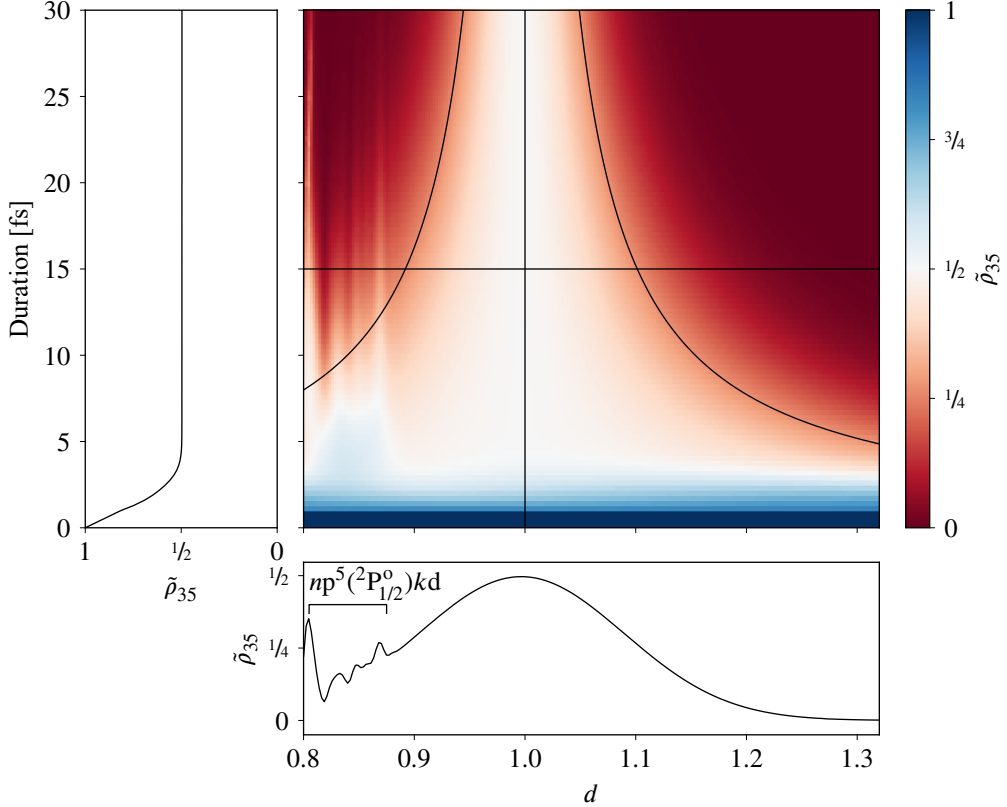


FIGURE 4: Degree of coherence as a function of pulse duration (FWHM of temporal intensity profile) and detuning ratio d . The hyperbolas in the main panel indicate the ‘coherence bandwidth’ within which $\tilde{\rho}_{35} > (2\sqrt{e})^{-1}$. The black horizontal/vertical lines mark lineouts at constant duration/detuning ratio, which are shown in the lower/left panels. As the pulse duration exceeds the quantum beat period, the peaks become spectrally resolvable, and the total overlap at the central frequency becomes half of that at vanishing pulse duration. The peaks appearing below $d \approx 0.9$ occur when the lower harmonic excites autoionizing Rydberg states between $^2P_{3/2}$ and $^2P_{1/2}$ thresholds.

where $\tilde{c} \equiv c_2(t_a)/c_1(t_a)$ (this ratio is assumed to be constant with t_a ; i.e. it only depends on the relative photoionization cross-section) and $\Delta E \equiv E_2 - E_1$. The last factor expresses the fact that the periodic ionization does not introduce dephasing between the two substates, as long as

$$\Delta t = \frac{2\pi r}{\Delta E}, \quad (14)$$

is fulfilled, for any integer r . Δt is a multiple of the quantum beat period for an energy separation ΔE , which does not depend on the duration of the XUV pulse. In the spectral domain, this corresponds to requiring the final electron kinetic energy to be the same.

We introduce the *degree of coherence*:

$$\tilde{\rho}_{mn} \equiv \frac{|\rho_{mn}|}{\sqrt{\rho_{mm}\rho_{nn}}}, \quad (15)$$

which normalizes the coherence between two ions to their respective populations. Figure 4 shows the degree of coherence, as a function of XUV pulse duration and detuning ratio. For short pulse durations, this quantity is larger than $\frac{1}{2}$ (left panel of figure 4). In this regime, the interaction with

the XUV pulse occurs within one quantum beat period (3.2 fs), and the four pathways indicated in figure 2 into the continuum have a partial spectral overlap. For larger pulse durations, two of the pathways become distinguishable, and do not contribute to the coherence between the ionic substates. The two remaining pathways, namely via $\Omega_<$ leaving the ion in ${}^2\text{P}_{3/2}^o$, and via $\Omega_>$ leaving the ion in ${}^2\text{P}_{1/2}^o$, cannot be distinguished when measuring the photo-electron, provided the resonance condition $d = 1$ is met. The maximum degree coherence is $\frac{1}{2}$. If $d \neq 1$, complete decoherence occurs in the long-pulse limit.

4 IONIZATION BY AN ATTOSECOND PULSE TRAIN

We consider now the effect of ionization with an attosecond pulse train, by including additional harmonic components. To focus on this aspect of the problem, we use a simplified model, where the dipole matrix elements for ionization are replaced with Heaviside functions (this is an approximation of a flat continuum, i.e. no resonances present):

$$z(\varepsilon) = \theta(\varepsilon), \quad (16)$$

where ε , as before, is the energy of the continuum electron. We still use the *Ansatz* (4), albeit with a compact notation only considering different channels n :

$$|\Psi(t)\rangle = c_0(t)|\Psi_0\rangle + \sum_n \int d\varepsilon c_n(t; \varepsilon)|n\varepsilon\rangle. \quad (17)$$

Inserting this in the Schrödinger equation and applying first-order time-dependent perturbation theory (i.e. the ground state is unaffected by the weak-field ionization; $c_0(t) = 1$), the solution reads

$$c_n(t) = -i\theta(\varepsilon) \int_{-\infty}^t dt' \mathcal{E}(t') \exp(iEt'). \quad (18)$$

Evaluating at the time of measurement ($t = +\infty$), we see that the coefficient becomes the Fourier transform of the driving field, evaluated at $-E_n - \varepsilon$. From this, we get the coherence between two channels (m, n) as

$$\rho_{mn} = - \int d\varepsilon \theta(\varepsilon) \hat{\mathcal{E}}^*(E_m + \varepsilon) \hat{\mathcal{E}}(-E_n - \varepsilon), \quad (19)$$

where $\hat{\mathcal{E}}(\omega)$ designates the Fourier transform of $\mathcal{E}(t)$. This expression shows that the coherence primarily arises from a correlation of the field with itself shifted by the energy difference $E_m - E_n$.

We will now apply (19) to the case of driving fields consisting of harmonic orders $q \in [q_1, q_2]$. Assuming $q_1\omega_0, q_2\omega_0 > E_m, E_n$, i.e. all constituent harmonic orders reach above both ionization thresholds, we have in total $2(\Delta q + 1)$ pathways into the continuum, where $\Delta q = q_2 - q_1$. In the case of resonance, $d = 1$, $2\Delta q$ of these pathways will overlap, which means, in the long-pulse limit,

$$\tilde{\rho}_{mn} = \frac{\Delta q}{\Delta q + 1}, \quad (20)$$

which of course tends to unity with increasing bandwidth. This is illustrated in figure 5 for the case of five harmonics; the maximum degree of coherence is indeed $\frac{1}{5}$, which occurs at $d = 1$.

Figure 5 also serves the purpose of illustrating the generalization of the quantum beat condition (14); e.g. the case $r = 2$ corresponds in the time domain to ionizing pulses arriving every other

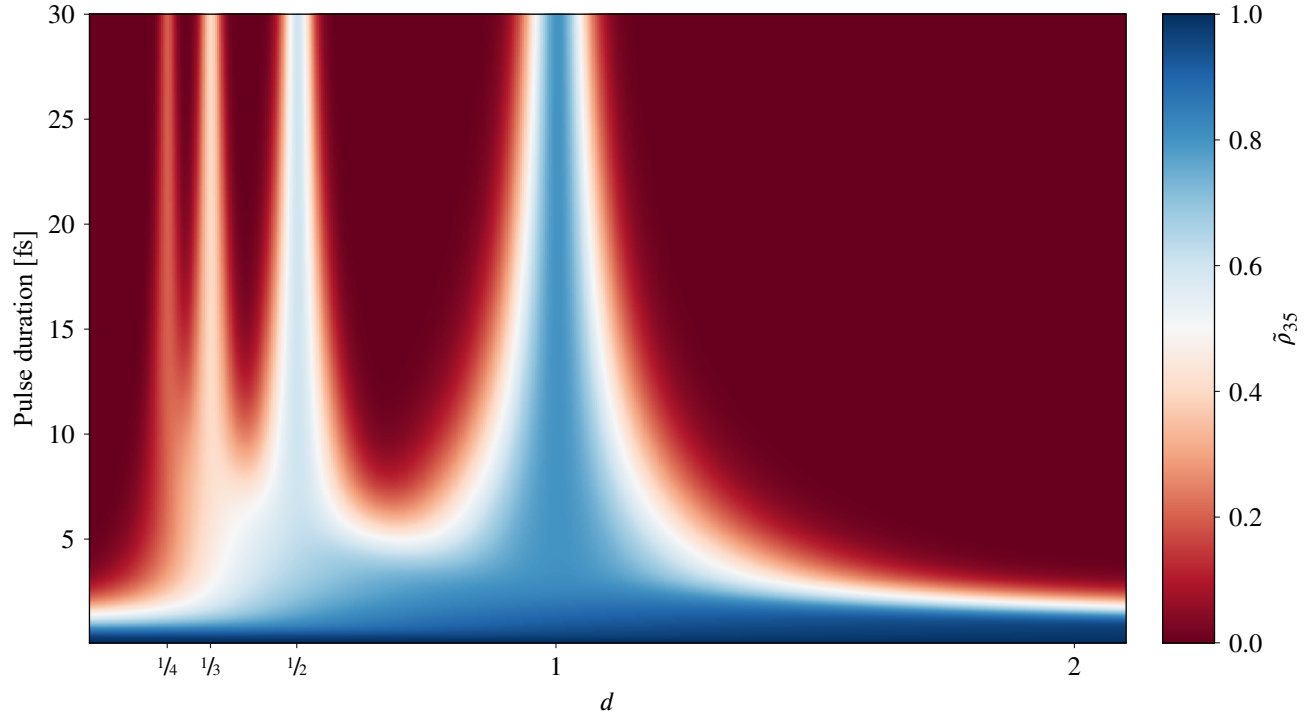


FIGURE 5: The effect of using five harmonics: At $d = 1$, 4 harmonics out of 5 will yield photo-electron peaks that overlap with those shifted by the spin-orbit splitting. The peaks appearing at $d = 1/4, 1/3, 1/2$ correspond to 1, 2, and 3 harmonics resulting in overlapping photo-electron peaks, respectively. In the time domain, this corresponds to ionizing pulses arriving at every $r = 4, 3, 2$ quantum beat periods.

quantum beat period. Such a field can be realized through red-blue HHG (resulting in odd *and* even harmonic orders) from a fundamental frequency $\Delta E_{\text{s-o}}/2$ (for Xe with $\Delta E_{\text{s-o}} \approx 1.3 \text{ eV}$, a fundamental driving wavelength $\lambda \approx 1.9 \mu\text{m}$ would thus be necessary). From this we see that in the spectral domain, the generalized quantum beat condition (14) is simply $d = 1/r$, $r \in \mathbb{Z}$.

Finally, we have also checked that in the long-pulse limit, the case of $d = 1/2$, using only odd-order harmonics is no different from the case of $d = 1$, using even- and odd-order harmonics. Thus the change of parity (phase difference) of consecutive pulses in the attosecond pulse train has no impact on the coherence, and we conclude that the degree of coherence is essentially dictated by the amount of indiscernible pathways.

5 CONCLUSION

In summary, we have shown that it is possible to induce coherence between two ionic substates using pulses of duration longer than the quantum beat time of their superposition. This is possible, provided a resonance condition is fulfilled, namely that the driving field has at least two frequency components spaced by precisely the energy difference of the levels of interest. This result shows that when the electron wave packets arising from different pathways have the same kinetic energy, we cannot know which way the ionization occurred. This situation is reminiscent of a Young's double slit experiment [see for instance Arndt et al. (2005)], with the two harmonic orders playing the roles of the two slits. It has to be noted, however, that no interference can be detected in the photo-electron signal, unless the ions are brought to the same final state via some mechanism

[e.g. Goulielmakis et al. (2010) did this by further exciting from the fine structure superposition using an XUV pulse]. Otherwise, it would be possible to detect the ions and the photo-electrons in coincidence mode and establishing the ionization pathway.

6 ACKNOWLEDGMENTS

We acknowledge the help of Oleg Zatsarinny, and would like to thank Andreas Buchleitner, Andreas Wacker, Kevin Dunseath, Mikhail Ivanov, Tobias Brünner, and Tomas Brage for fruitful discussions. This work was supported by the Swedish Foundation for Strategic Research, the Swedish Research Council, the Knut and Alice Wallenberg Foundation, the European Research Council (PALP), and by funding from the NSF under grant PHY-1307083.

REFERENCES

Alvermann, A., Fehske, H., and Littlewood, P. B. (2012). ‘Numerical time propagation of quantum systems in radiation fields’. *New Journal of Physics* **14**.10, p. 105008. DOI: [10.1088/1367-2630/14/10/105008](https://doi.org/10.1088/1367-2630/14/10/105008).

Arndt, M., Hornberger, K., and Zeilinger, A. (2005). ‘Probing the limits of the quantum world’. *Physics World* **18**.3, pp. 35–40. DOI: [10.1088/2058-7058/18/3/28](https://doi.org/10.1088/2058-7058/18/3/28).

Cowan, R. (1981). *The theory of atomic structure and spectra*. Berkeley: University of California Press. ISBN: [0520038215](https://doi.org/10.520038215).

Froese Fischer, C., Tachiev, G., Gaigalas, G., and Godefroid, M. R. (2007). ‘An MCHF atomic-structure package for large-scale calculations’. *Computer Physics Communications* **176**.8, pp. 559–579. DOI: [10.1016/j.cpc.2007.01.006](https://doi.org/10.1016/j.cpc.2007.01.006).

Goulielmakis, E., Loh, Z.-H., Wirth, A., Santra, R., Rohringer, N., Yakovlev, V. S., Zherebtsov, S., Pfeifer, T., Azzeer, A. M., Kling, M. F., Leone, S. R., and Krausz, F. (2010). ‘Real-time observation of valence electron motion’. *Nature* **466**.7307, pp. 739–743. DOI: [10.1038/nature09212](https://doi.org/10.1038/nature09212).

Klünder, K., Johnsson, P., Swoboda, M., L’Huillier, A., Sansone, G., Nisoli, M., Vrakking, M. J., Schafer, K. J., and Mauritsson, J. (2013). ‘Reconstruction of attosecond electron wave packets using quantum state holography’. *Physical Review A* **88**.3, p. 033404. DOI: [10.1103/PhysRevA.88.033404](https://doi.org/10.1103/PhysRevA.88.033404).

Kurka, M., Rudenko, A., Foucar, L., Kühnel, K., Jiang, Y., Ergler, T., Havermeier, T., Smolarski, M., Schössler, S., Cole, K., et al. (2009). ‘Two-photon double ionization of Ne by free-electron laser radiation: a kinematically complete experiment’. *Journal of Physics B: Atomic, Molecular and Optical Physics* **42**.14, p. 141002.

Landau, L. D. and Lifshitz, E. M. (1977). *Quantum mechanics : non-relativistic theory*. 3rd. Vol. 3. Course of Theoretical Physics. Oxford New York: Pergamon Press. ISBN: [978-0-08-020940-1](https://doi.org/10.520038215).

Magnus, W. (1954). ‘On the exponential solution of differential equations for a linear operator’. *Communications on Pure and Applied Mathematics* **7**.4, pp. 649–673. DOI: [10.1002/cpa.3160070404](https://doi.org/10.1002/cpa.3160070404).

Mauritsson, J., Remetter, T., Swoboda, M., Klünder, K., L’Huillier, A., Schafer, K. J., Ghafur, O., Kelkensberg, F., Siu, W., Johnsson, P., Vrakking, M. J. J., Znakovskaya, I., Uphues, T., Zherebtsov, S., Kling, M. F., Lépine, F., Benedetti, E., Ferrari, F., Sansone, G., and Nisoli, M. (2010). ‘Attosecond Electron Spectroscopy Using a Novel Interferometric Pump-Probe Technique’. *Physical Review Letters* **105** (5), p. 053001. DOI: [10.1103/PhysRevLett.105.053001](https://doi.org/10.1103/PhysRevLett.105.053001).

Nikolopoulos, L. A. A. (2013). ‘Time-Dependent Theory of Angular Correlations in Sequential Double Ionization’. *Physical Review Letters* **111**.9. DOI: [10.1103/physrevlett.111.093001](https://doi.org/10.1103/physrevlett.111.093001).

Pabst, S., Greenman, L., Ho, P. J., Mazziotti, D. A., and Santra, R. (2011). ‘Decoherence in Attosecond Photoionization’. *Physical Review Letters* **106**.5. DOI: [10.1103/physrevlett.106.053003](https://doi.org/10.1103/physrevlett.106.053003).

Pabst, S., Lein, M., and Wörner, H. J. (2016). ‘Preparing attosecond coherences by strong-field ionization’. *Physical Review A* **93**.2. DOI: [10.1103/physreva.93.023412](https://doi.org/10.1103/physreva.93.023412).

Saad, Y. (1992). ‘Analysis of some Krylov subspace approximations’. *SIAM Journal on Numerical Analysis*.

Salour, M. and Cohen-Tannoudji, C. (1977). ‘Observation of Ramsey’s interference fringes in the profile of Doppler-free two-photon resonances’. *Physical Review Letters* **38**.14, p. 757. DOI: [10.1103/PhysRevLett.38.757](https://doi.org/10.1103/PhysRevLett.38.757).

Teets, R., Eckstein, J., and Hänsch, T. (1977). ‘Coherent two-photon excitation by multiple light pulses’. *Physical Review Letters* **38**.14, p. 760.

Tzallas, P., Skantzakis, E., Nikolopoulos, L. A. A., Tsakiris, G. D., and Charalambidis, D. (2011). ‘Extreme-ultraviolet pump–probe studies of one-femtosecond-scale electron dynamics’. *Nature Physics* **7**.10, pp. 781–784. DOI: [10.1038/nphys2033](https://doi.org/10.1038/nphys2033).

Zatsarinny, O. (2006). ‘BSR: *B*-spline atomic *R*-matrix codes’. *Computer Physics Communications* **174**.4, pp. 273–356. DOI: [10.1016/j.cpc.2005.10.006](https://doi.org/10.1016/j.cpc.2005.10.006).

Zatsarinny, O. and Froese Fischer, C. (2009). ‘Atomic structure calculations using MCHF and BSR’. *Computer Physics Communications* **180**.11, pp. 2041–2065. DOI: [10.1016/j.cpc.2009.06.007](https://doi.org/10.1016/j.cpc.2009.06.007).